Appl Phys B (2009) 97: 53–60
DOI 10.1007/s00340-009-3531-y

Applied Physics B
Lasers and Optics

Dispersionless saturable absorber mirrors with large modulation depths and low saturation fluences

M.P. Lumb · P.N. Stavrinou · E.M. Clarke · R. Murray · C.G. Leburn · C. Jappy · N.K. Metzger · C.T.A. Brown · W. Sibbett

Received: 16 February 2009 / Revised version: 23 March 2009 / Published online: 2 May 2009

Abstract We show that it is possible to eliminate group delay dispersion over wide bandwidths in low-finesse, resonant saturable absorber mirrors, whilst maintaining a low saturation fluence and a high modulation depth. By modelling the mirror structure we demonstrate that these properties can be produced by capping a resonant device with a single dielectric layer of carefully selected refractive index. We show that a specially capped dispersionless structure minimises the temporal broadening of femtosecond pulses reflected from the mirror. We compare this device against uncapped-resonant and anti-resonant structures. The superior performance of the capped, dispersionless device was verified experimentally by comparing resonant, anti-resonant and dispersionless quantum-dot (QD) saturable absorber mirrors incorporated into a Cr^{4+}:forsterite laser system. We found that a minimum pulse duration of 86 fs could be achieved for the dispersionless structure at 1290 nm with an output power of 55 mW compared to 122 fs in an anti-resonant structure and several-picosecond pulses for a resonant structure.

PACS 42.60.Fc · 78.67.Pt · 78.67.Hc

M.P. Lumb (✉) · P.N. Stavrinou · E.M. Clarke · R. Murray
Department of Physics, Blackett Laboratory, Imperial College London, London, SW7 2BW, UK
e-mail: matthew.lumb05@imperial.ac.uk
Fax: +44-20-75942077

C.G. Leburn · C. Jappy · N.K. Metzger · C.T.A. Brown · W. Sibbett
J.F. Allen Physics Research Laboratories, School of Physics and Astronomy, University of St. Andrews, St. Andrews, KY16 9SS, Scotland, UK

1 Introduction and structure design

Semiconductor saturable absorber mirrors (SESAMs) are simple yet effective devices that can be used in the production of ultra-short pulses by passive mode locking in a variety of lasers. A SESAM typically consists of a distributed Bragg reflector (DBR) incorporating an absorbing element, the saturation of which leads to the mirror having intensity dependent reflectivity [1]. This paper concentrates on the low-finesse, resonant SESAM design [2, 3], where the absorber region is situated in a resonant cavity formed between the DBR and the upper surface of the device. Simple post-growth techniques, such as chemical etching [4] and dielectric capping [3], can be used to modify the basic resonant cavity and therefore adjust the important SESAM properties. We compare the basic low-finesse, resonant design with two modified designs derived from this structure; the resonant cavity with the addition of a lower-index dielectric encapsulant layer, and a structure where the cavity has been etched to anti-resonance. Through detailed modelling of the capped structure, we have found that the phase dispersion of the SESAM is highly sensitive to the choice of cap layer index, and in Sect. 2 of this paper we describe how it is possible to entirely eliminate the phase dispersion of the SESAM over wide bandwidths using only a single dielectric cap layer of carefully selected index. Furthermore, we demonstrate that the choice of cap layer index and resonant cavity length provides a design route to dispersionless SESAMs having low saturation fluences and large modulation depths. An experimental verification of these findings is presented in Sect. 5, where the basic resonant structure, the etched anti-resonant structure and the capped dispersionless structure had been integrated into a Cr^{4+}:forsterite laser configuration, and a significant performance improvement was observed for the

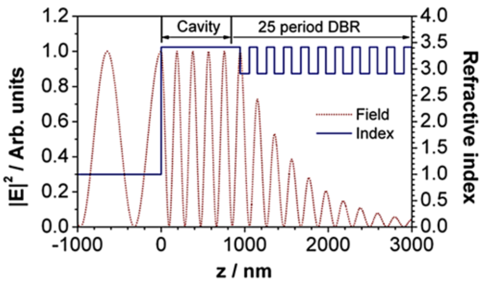

Fig. 1 The refractive index profile and square of the electric field amplitude at the design wavelength for the low-finesse, resonant SESAM

capped dispersionless device when compared to the resonant and anti-resonant devices.

The DBR consists of alternate $\lambda_0/4$ thick layers of high and low refractive indices, where λ_0 is the design wavelength, corresponding to the centre of the high-reflectivity stop-band region in the frequency domain. An exemplar resonant structure is displayed in Fig. 1, with a $9\lambda_0/4$ cavity region and a 25 period AlAs/GaAs DBR grown on a GaAs substrate and this was modelled using a standard transfer matrix technique [5, 6]. The refractive indices of GaAs and AlAs are interpolated to literature values and λ_0 is taken to be 1290 nm. Absorber layers, such as quantum wells or, in more recent devices, InAs quantum dots [7–9], are usually positioned at the antinodes of the field inside the cavity, shown in Fig. 1. The impact of typically thin, weakly absorbing layers with low index contrast on the phase shift on reflection from the mirror can be neglected for the purposes of this work.

The ratio of the peak square field amplitude inside the cavity region to that in air is known as the enhancement factor [3, 4], $\xi(\lambda)$. At the design wavelength, the peak field intensity inside the cavity region of the low-finesse, resonant device in Fig. 1 is equal to the peak field in air and therefore $\xi(\lambda_0)$ is unity for this design. A large ξ leads to a low saturation fluence, E_{sat}, and large modulation depth, ΔR. Low E_{sat} can help to produce stable, CW mode locking [10], particularly in systems where the intra-cavity pulse energy is low. Sufficient ΔR is also necessary for pulse-shaping mechanisms to operate efficiently [11] but too large a value of ΔR can introduce losses into the laser cavity too great to sustain laser operation [2]. Therefore, the sample design and choice of absorber needs to be well matched to the particular requirements of the intended laser system.

2 Group delay dispersion and third-order dispersion

The complex reflection amplitude of the entire structure, $r(\omega)$, can be written in polar form and in the frequency domain is defined as [6]

$$r(\omega) = \frac{E^-_{\text{air}}}{E^+_{\text{air}}} = \rho(\omega)\exp\bigl[i\phi(\omega)\bigr]. \quad (1)$$

Here E^+_{air} and E^-_{air} are the amplitudes of the forward and reverse propagating fields in air, respectively. The magnitude of the complex reflection coefficient is $\rho(\omega)$ and $\phi(\omega)$ is the phase shift on reflection from the mirror. In femtosecond lasers, an important parameter governing the attainable pulse duration is the group delay dispersion (GDD) [12], which is given by the second derivative of the phase shift on reflection, $\phi''(\omega)$. In the case of a resonant structure the GDD is zero at the resonant frequency of the cavity (ω_0) but otherwise varies sharply either side of ω_0. This type of response around ω_0 places a limit on the minimum pulse duration that can be obtained. The key requirement for ultrashort pulse formation is for the GDD response to remain flat over a suitably broad bandwidth centred around ω_0 [13]. Although low-finesse resonant structures have the advantage of a large enhancement factor, the sharply varying GDD around ω_0 does not allow the formation and preservation of subpicosecond pulses within a laser cavity. The investigation of possible additions to the basic cavity design with complementary experimental assessments formed the subject matter of this work.

In order to modify the GDD in the vicinity of ω_0, several post-growth cavity modification techniques are available, including chemical etching [4], post-growth capping [3] or tilting of the structure [14]. Deposition of an additional $\lambda_0/4$ GaAs cap, or removal of a $\lambda_0/4$ GaAs layer, reverses the resonance condition at $\lambda_0(\omega_0)$ from resonant to anti-resonant, suppressing the dispersion across the stop-band region but also lowering $\xi(\lambda_0)$ to a value of $(n_{\text{air}}/n_{\text{GaAs}})^2$, which at 1290 nm is 0.086. However, Spuhler et al. [3] have shown that a quarter-wave cap of lower index material on the front surface of a low-finesse resonant sample partially suppresses the GDD variation across the stop-band region without reducing $\xi(\lambda_0)$ to the extent of an anti-resonantly designed structure.

To describe the flatness of the GDD curves for these devices it is useful to define a property called the GDD flatness bandwidth (GFB), which is the bandwidth around the design wavelength over which the absolute value of GDD remains within a fixed bound, X. For the resonant structure with a quarter-wave cap the GDD(ω_0) is also zero. The GFB is then defined as GFB $= 2|\omega_X - \omega_0|$ where ω_X is the closest frequency to ω_0 at which the GDD exceeds X. Close to ω_0 the GDD(ω) is approximately linear and for small X,

$$\text{GFB} = \frac{2X}{|\phi'''(\omega_0)|}. \quad (2)$$

Here $\phi'''(\omega_0)$ is the third-order dispersion (TOD) at the design frequency. Equation (2) breaks down at $\phi'''(\omega_0) = 0$ since the GFB is limited by the extent of the stop-band, but it does show that the TOD is the important factor for minimising the pulse broadening from the mirror. The GFB and TOD for a dispersion bound of $X = 50$ fs^2 for $\lambda_0/4$

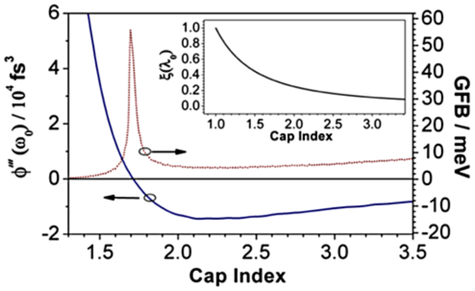

Fig. 2 The third-order dispersion and GDD flatness bandwidth for the SESAM with quarter-wave caps of different refractive index. *Inset*: The enhancement factor at the design wavelength for different quarter-wave cap indices

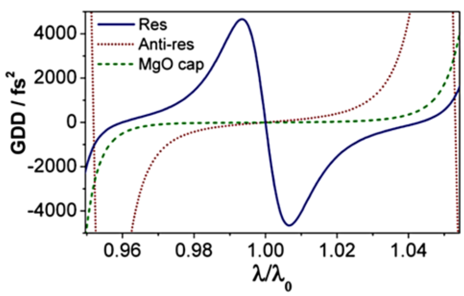

Fig. 3 The GDD curves for the uncapped low-finesse, resonant sample (*solid blue line*), with an $n = 1.71$ quarter-wave cap (*dashed green line*) and with a quarter-wave GaAs cap (*dotted brown line*)

caps of different index are displayed in Fig. 2. The peak in GFB as the TOD passes through zero is clear, and this occurs for a cap index of 1.71. Also, $\xi(\lambda_0)$ is increased for decreasing cap indices, shown in the inset to Fig. 2, which shows the enhancement factor at λ_0 as a function of the index of the quarter-wave cap. To maintain a high modulation depth and low saturation fluence it is therefore favourable to keep the quarter-wave cap index low. In fact, for $X = 50$ fs^2 and an $n = 1.71$ quarter-wave cap, the GFB is more than seven times larger than that for an anti-resonant SESAM and $\xi(\lambda_0) = 0.338$, approximately a factor of four greater. The GDD curves for the uncapped resonant structure, the $n = 1.71$ quarter-wave capped structure and the $n = n_{\mathrm{GaAs}}$ quarter-wave capped (anti-resonant) structure as displayed in Fig. 3, demonstrate the broad-band elimination of GDD in the capped device.

The cavity can be approximated as a basic Gires–Tournois (GT) interferometer with the DBR forming a high-reflectivity interface and the other interface formed by the upper surface of the cavity and air. Previous considerations by Moenster et al. [13] have shown that GDD and TOD vanish if the reflectivity of the top surface is coated with a perfect anti-reflection coating, as the multiple reflections within the cavity are suppressed. For a GT interferometer with a GaAs spacer, an anti-reflecting upper interface and a high-reflector lower interface yields a value of $\xi(\lambda_0) = n_{\mathrm{air}}/n_{\mathrm{GaAs}} = 0.293$. The simplest anti-reflection coating for GaAs is a quarter-wave cap layer where the cap index is given by $n = \sqrt{n_{\mathrm{air}} n_{\mathrm{GaAs}}} = 1.85$ at 1290 nm [15]. However, it is surprising to find that the zero TOD condition for the capped low-finesse resonant structure does not occur for a single anti-reflection coating layer of index $n = 1.85$, but instead TOD passes through zero for an $n = 1.71$ quarter-wave cap. The reason for this is twofold: the reflectance of the coated GaAs is non-zero for frequencies either side of ω_0 and also the DBR has phase dispersion around ω_0 [16, 17], both of which are important when the cavity is thin and the phase shift accrued on one round trip of the cavity is small. Importantly, as shown in the inset to Fig. 2, using an $n = 1.71$ quarter-wave cap layer gives a 15% improvement in $\xi(\lambda_0)$ over a perfect anti-reflection-coated structure whilst still achieving zero TOD. Such capping produces not only a performance improvement but also reduces the technical complexity of the post-growth coating required.

3 Pulse broadening

To demonstrate the pulse broadening effect from the phase shift on reflection, in the absence of any pulse shaping mechanisms, the spectrum of pulses reflected from the mirror was evaluated. A transform-limited Gaussian incident pulse field was described by $E_i(t) = A_0 \exp(-t^2/4\sigma_i^2) \exp(i\omega_0 t)$, with ω_0 and σ_i the design frequency of the mirror and the incident RMS pulse duration, respectively. Using the autocorrelation theorem, the field of the reflected pulse, $E_r(t)$, is obtained from the Fourier transform of the product of the incident pulse spectrum and the mirror reflection amplitude as described in [18, 19], and the reflected pulse intensity is described by $I_r(t) \propto |E_r(t)|^2$. The RMS pulse duration of the reflected pulse σ_r is calculated from the first and second moments of $I_r(t)$ as described in [18–20]. The broadening ratio, σ_r/σ_i, is shown in Fig. 4 for $\sigma_i = 25$ fs pulses incident on the mirror and is a minimum at the cap index giving zero TOD. An RMS pulse duration of 25 fs corresponds to a FWHM pulse width of $\sim$59 fs. This shows that a wide GFB is essential if the broadening of sub-picosecond pulses is to be minimised. For RMS durations shorter than 25 fs, the pulse spectrum penetrates further into the lower reflectivity, highly dispersive fringes either side of the stop-band. Consequently the pulses become severely distorted and an appreciable fraction of the incident pulse energy is lost. It follows, therefore, that the pulse duration is ultimately limited by the finite extent of the stop-band, as reported by other authors [21].

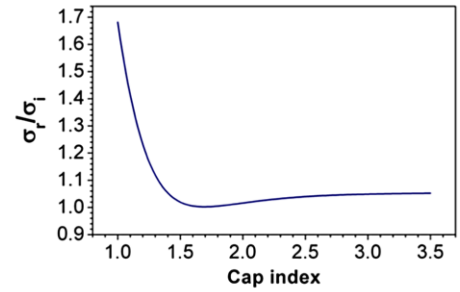

Fig. 4 The ratio of the RMS duration of the reflected to incident pulses for $\sigma_i = 25$ fs Gaussian pulses incident on the SESAM

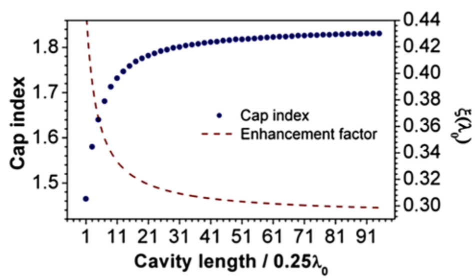

Fig. 5 The quarter-wave cap index required for zero TOD and the resulting enhancement factor at the design wavelength

4 Cavity length considerations

The discussion thus far has concentrated on the particular case of a $9\lambda_0/4$ resonant cavity device, but Fig. 5 shows that the quarter-wave cap index required to achieve $\mathrm{TOD}(\omega_0) = 0$ is a function of the resonant cavity thickness. The cavity thicknesses plotted in Fig. 5 are odd multiples of $\lambda_0/4$ to satisfy the condition of resonance at λ_0. The enhancement factor $\xi(\lambda_0)$ is also plotted for the cap indices required to achieve zero TOD. For very short cavities, the index required for dispersionless operation is very low, which means the enhancement factor of this structure is high. As the cavity is lengthened, the index required to achieve dispersionless operation tends towards the anti-reflection condition of $n = 1.85$, as the contribution to the dispersion from the DBR and the cap become small in comparison to the resonant-cavity dispersion. Therefore, to ensure high enhancement factor, dispersionless SESAMs, the resonant cavity length should be kept as short as possible. However, a short cavity length does place restrictions on the amount of absorber material that can be incorporated into the structure, and this represents a further design consideration for SESAMs used for femtosecond pulse generation.

5 Experimental investigation

To demonstrate the effect of eliminating dispersion on the performance of the SESAM in a laser cavity, a test device

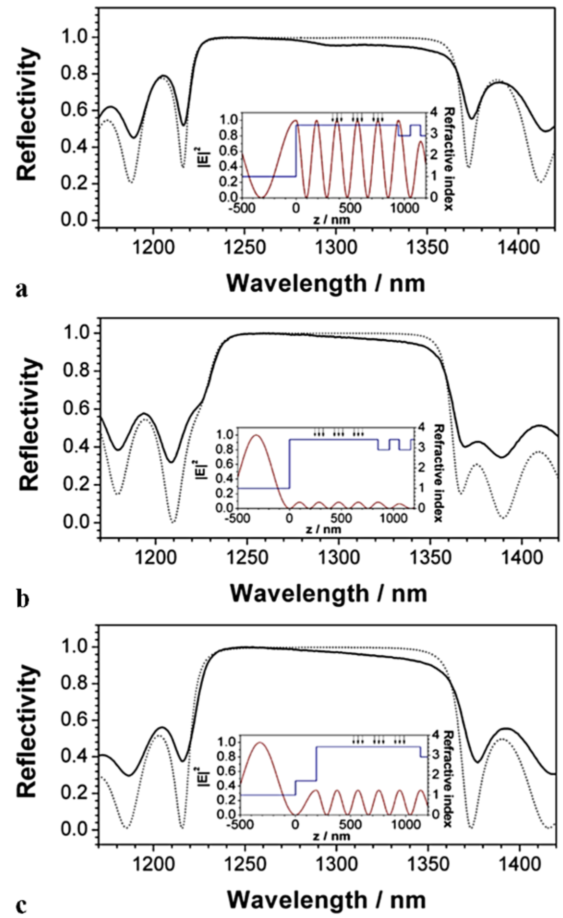

Fig. 6 The measured (*solid lines*) and calculated (*dotted lines*) reflectivity for (**a**) the uncapped resonant, (**b**) anti-resonant and (**c**) MgO capped structures. The insets illustrate the refractive index profile and field standing wave pattern at 1290 nm. The arrows denote the position of the QD layers

was grown. The device was based on the design illustrated in Fig. 1, with nine absorbing InAs quantum-dot layers incorporated into a $9\lambda_0/4$ GaAs cavity. The dot absorber layers were positioned in three groups of three, with each group centred around antinodes of the field in the cavity on resonance, with the layers each separated by 40 nm GaAs spacer layers. The positions of these dots are displayed on the inset to Fig. 6a, which shows the nominal refractive index profile for the resonant SESAM and the calculated field structure.

As in previous work [4], the contribution to the overall cavity thickness from the dot layers was found to lengthen the cavity slightly. The extra cavity thickness contribution was found to be equivalent to a GaAs thickness of 14 nm, which was corrected by chemical etching of the cavity using a 2:1 solution of H_2O_2 and citric acid for two minutes with an etch rate of 7.0 ± 0.2 nm/min. Figure 6a shows that the reflectivity profile of the etched sample and the calculated reflectivity pattern of the nominal resonant structure are in good agreement. The reflectivity measurements were made using an optical microscope connected to an optical spec-

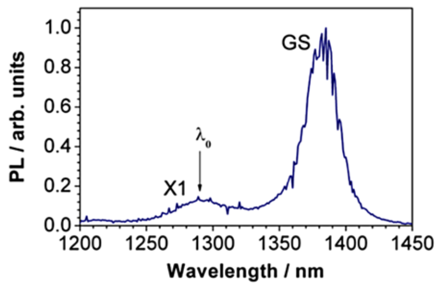

Fig. 7 Room temperature photoluminescence measurements of a single layer of QDs incorporated into the SESAM, with peak X1 emission at 1290 nm. Note that the GS peak coincides with atmospheric water absorption

trum analyser (OSA), with illumination from a broad-band lamp. The spectra were calibrated using a gold mirror. In the stop-band region, a slight dip is visible on resonance due to the absorption in the dot layers. There is a small linear variation in the measured reflectivity across the stop-band which is a feature of a wavelength dependence of the gold reflectivity, and the reflectivity minima of the SESAMs were measured to be slightly greater than the calculated curves due to the resolution limit of the OSA and a small amount of incoherent back-reflection from the substrate, which was not included in the calculation.

An anti-resonant structure was formed by etching a further $\lambda_0/4$ layer from the resonant structure, which corresponded to an etch duration of 13.5 min. The inset to Fig. 6b shows the nominal refractive index profile of the anti-resonant device and the position of the dots, and also shows the reduction in $\xi(\lambda_0)$ compared with the resonant sample. The measured reflectivity was fitted using a cavity thickness of 771 nm. Finally, the resonant structure was capped with a nominal 189 nm layer of MgO, which has a refractive index of 1.71 in the region around 1290 nm. The nominal refractive index profile is demonstrated in the inset to Fig. 6c and the calculated reflectivity pattern is also in good agreement with the measured normal incidence reflectivity spectrum.

The devices were grown by solid-source molecular beam epitaxy (MBE). The dots have an areal density of 1.6×10^{10} cm^{-2} per layer, and are designed to have the first excited state (X1) transition resonant with λ_0 at 295 K. The dot layers are long wavelength bi-layers [22] consisting of a seed layer of QDs and a second QD layer separated by 10 nm. The seed layer was grown by deposition of 2.4 ML InAs at 0.014 MLs^{-1} at a substrate temperature of 492°C. The second QD layer was grown by deposition of 3.3 ML InAs, also at 0.014 MLs^{-1}, at a substrate temperature of 467°C. The seed layer and 10 nm GaAs spacer layer was included in the GaAs buffer between each second layer of the bi-layers. However, the state energies of the seed layer dots reside at much shorter wavelengths than 1290 nm and therefore do not participate in the absorption. Room temperature photoluminescence measurements on a nominally identical sample of dots, grown without the DBR, are displayed in Fig. 7, showing the X1 transition at room temperature peaks close to 1290 nm. The several advantages of QDs as absorbers in SESAMs include: wide inhomogeneous linewidths, fast carrier dynamics of dot transitions [23], and the potential for low saturation fluences [24] due to the three-dimensional carrier confinement. Furthermore, the modulation depth of QD-SESAMs can be controlled by the areal density of the QDs [25]. QDs are also highly suited to the 1290 nm spectral region, avoiding the need for post-growth annealing procedures required with GaInNAs based devices [26, 27]. Choosing the X1 transition as the absorptive transition offers the possibility of faster recovery dynamics [14] and larger modulation depths [4] over traditional ground state devices.

A Cr^{4+}:forsterite laser comprising of a four-mirror asymmetric, astigmatically compensated Z-fold cavity was constructed to assess the mode locking capability of the SESAM devices. Other authors [28, 29] have suggested that with a SESAM in place the mode locking is operating in the soliton regime, with the SESAM assisting and stabilizing the mode locking. A schematic diagram of the laser configuration is shown in Fig. 8. The choice of a highly asymmetric laser cavity design allowed the laser cavity beam waist on the SESAMs to be controlled with a high degree of accuracy. This laser cavity geometry also allowed variation of the cavity beam size inside the gain medium, thus ensuring good overlap of the pump beam with the cavity beam and maximising the efficiency of laser output. The two folding mirrors M1 and M2 had radii of curvature of -100 and -75 mm, respectively. These mirrors were designed for high transmissivity at the pump wavelength (1064 nm), and high reflectivity at wavelengths from 1250 to 1370 nm. A wedged output coupler with 0.5% coupling efficiency and a quantum-dot SESAM (or high reflection mirror) terminated the long and short arms of the four-mirror laser cavity. The gain medium was a 11.6 mm long Brewster-cut Cr^{4+}:forsterite crystal with a small-signal pump absorption coefficient of 1.3 cm^{-1} and this was mounted in a water-cooled copper jacket maintained at a temperature of 15°C. The gain crystal was optically pumped by a *Spectra-Physics* Nd:YVO_4 laser, capable of delivering an output of up to 10 W of continuous wave near-diffraction-limited 1064 nm laser radiation. A simple telescope system and focusing lens were used to provide a $1/e^2$ pump beam spot radius of 35 µm in the gain crystal.

With the high-reflectivity mirror placed in the short arm continuous wave laser operation was possible. In this configuration, with the 0.5% output coupler in place, a maximum output power of 105 mW was achieved for an incident pump power of 5.1 W. The threshold for CW operation did

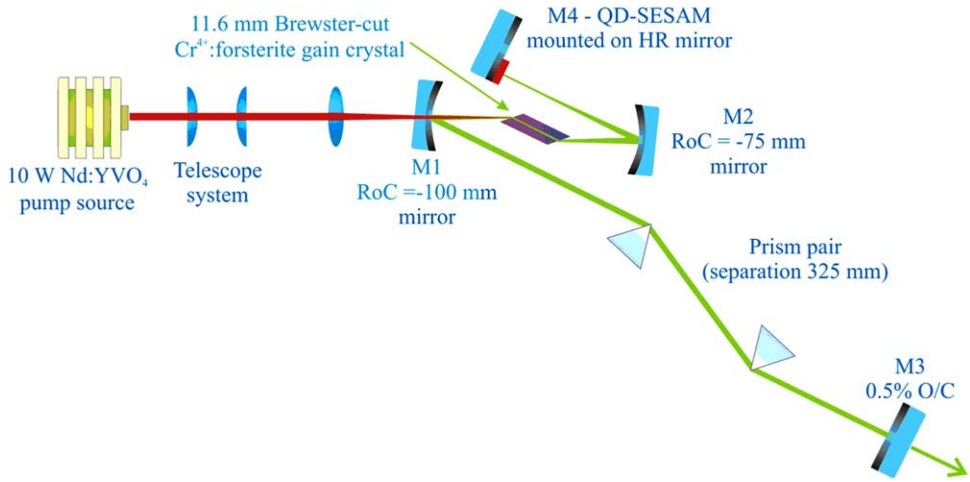

Fig. 8 Schematic of the self-starting mode-locked Cr^{4+}:forsterite laser resonator

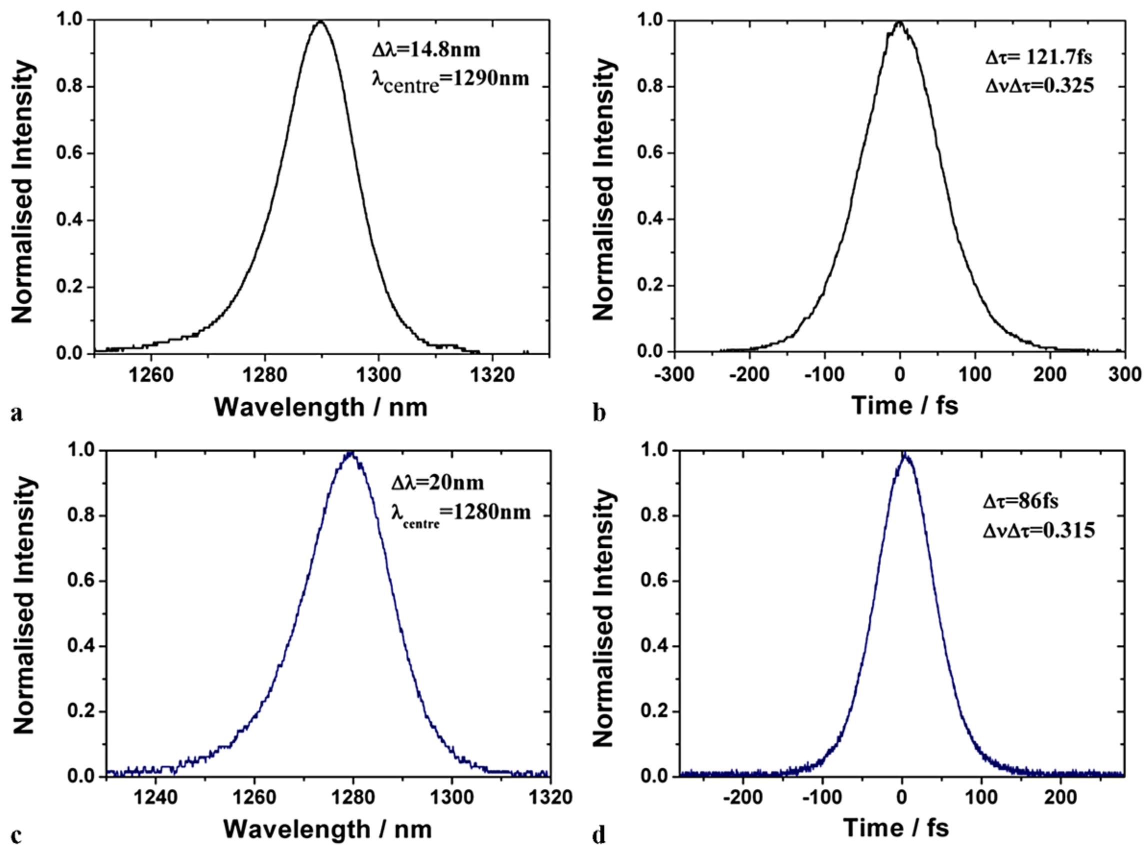

Fig. 9 (**a**) Measured optical spectrum and (**b**) corresponding intensity autocorrelation of the Cr^{4+}:forsterite laser with the anti-resonant QD-SESAM placed in the short arm of the laser cavity. (**c**) Measured optical spectrum and (**d**) corresponding intensity autocorrelation with the capped, resonant QD-SESAM

not increase significantly when the SESAMs were inserted (∼200 mW) implying low non-saturable losses for all of the SESAM devices assessed. The capped device did demonstrate slightly increased losses during high power CW operation, which could be due to losses in the MgO cap layer. (An investigation of alternative cap materials with similar refractive indices will be undertaken to identify suitable materials having minimal losses in a further study.)

Laser mode locking was obtained when the HR cavity mirror in the short arm of the cavity was replaced by each of the quantum-dot SESAMs. The intra-cavity beam incident on the SESAM had a radius of 200 µm. To generate pulses in the femtosecond domain two fused silica prisms with a tip–to–tip separation of 325 mm were inserted in the long arm of the laser cavity to provide the appropriate amount of negative dispersion compensation necessary to balance the positive dispersion of the Cr^{4+}:forsterite gain crystal.

With the uncapped resonant device in place it was possible to achieve self-starting pulsed operation, with a spectral bandwidth of 0.8 nm and peak wavelength of 1265.8 nm. A clear autocorrelation signal could not be obtained, probably due to the low peak power of the pulses, although the spectral bandwidth of these pulses implied a duration of several picoseconds. Adjustment of the dispersion compensating prisms did not shorten the pulse duration or improve the stability of the mode locking, implying that the pulse duration was limited by the large variation of GDD across the spectral bandwidth of this device.

Insertion of the anti-resonant device produced self-starting mode-locked operation with a spectral bandwidth of 14.8 nm and the FWHM pulse durations were 122 fs. The calculated time-bandwidth product of 0.325 implied that these were near-transform-limited pulses at the centre wavelength of 1290 nm assuming a sech^2 pulse intensity profile. The spectral profile and intensity autocorrelation trace are illustrated in Figs. 9a and 9b.

The threshold for mode locking with this device was observed to be when 4.5 W of pump light was incident on the gain crystal, corresponding to a fluence on the SESAM of 25 $\mu J/cm^2$. With the 0.5% output coupler in place, an average mode-locked output power of 40 mW was achieved.

Figures 9c and 9d show the spectral bandwidth and autocorrelation trace that was achieved with the capped resonant device in place. With this device it was possible to support a spectral bandwidth of 20 nm (Fig. 9c) at a centre wavelength of 1280 nm and the 86 fs pulses were 30% shorter than those in the anti-resonant case. The time-bandwidth product of 0.315 again implied the generation of near-transform-limited pulses. The reduction in the pulse duration supports the prediction of a minimum in pulse broadening on reflection from the capped device, shown in Fig. 4. However, the larger enhancement factor of this device may also contribute to the reduction in pulse duration due to the increased modulation depth. A maximum 55 mW of output power was generated with the 0.5% output coupler in place. The mode-locking threshold was measured for an incident pump power of 3.4 W which corresponds to a fluence of 17.5 $\mu J/cm^2$ incident upon the SESAM, and significantly this is 30% lower than that for the anti-resonant device due to the larger enhancement factor of the capped device and consequently lower saturation fluence.

6 Conclusion

We have found that for low-finesse, resonant semiconductor saturable absorber mirrors (SESAMs), quarter-wave cap indices can be selected to produce broad-band dispersionless structures having higher enhancement factors than structures with perfect anti-reflection coatings. These structures are a significant improvement in both enhancement factor and GDD flatness bandwidth over anti-resonant devices and eliminate the large GDD variations seen close to resonance in resonant devices. Dispersionless structures with high enhancement factors are especially beneficial for femtosecond lasers that require low saturation fluences and large modulation depths and these components have the additional benefits of simpler and cheaper processing than for multi-layer anti-reflection coatings. To demonstrate the improved properties of dispersionless quantum-dot SESAMs (QD-SESAMs), 86 fs transform-limited pulses have been generated from a Cr^{4+}:forsterite laser and this represents a 30% improvement over a sample that was etched to anti-resonance, and an order of magnitude improvement over the uncapped, resonant structure. The cap index required for dispersionless operation is found to be lower for shorter cavity lengths, heightening the effect and this has important implications on the design of resonant SESAMs for use in femtosecond pulse generation.

Acknowledgements The author would like to acknowledge the helpful contributions of Peter Spencer with the chemical etching and LaserOptik GmbH for the MgO deposition.

References

1. U. Keller, Nature **424**, 831 (2003)
2. U. Keller, K.J. Weingarten, F.X. Kartner, D. Kopf, B. Braun, I.D. Jung, R. Fluck, C. Honninger, N. Matuschek, J. Aus der Au, IEEE J. Sel. Top. Quantum Electron. **2**, 435 (1996)
3. G.J. Spuhler, K.J. Weingarten, R. Grange, L. Krainer, M. Haiml, V. Liverini, M. Golling, S. Schon, U. Keller, Appl. Phys. B **81**, 27 (2005)
4. M.P. Lumb, D.J. Farrell, E.M. Clarke, M.J. Damzen, R. Murray, Appl. Phys. B **94**, 393 (2009)
5. F. Abeles, Ann. Phys. **3**, 504 (1948)
6. O. Heavens, *Optical Properties of Thin Solid Films* (Butterworths, Stoneham, 1955)
7. A.A. Lagatsky, F.M. Bain, C.T.A. Brown, W. Sibbett, D.A. Livshits, G. Erbert, E.U. Rafailov, Appl. Phys. Lett. **91**, 231111 (2007)
8. E.U. Rafailov, S.J. White, A.A. Lagatsky, A. Miller, W. Sibbett, D.A. Livshits, A.E. Zhukov, V.M. Ustinov, IEEE Photonics Technol. Lett. **16**, 2439 (2004)
9. C. Scurtescu, Z.Y. Zhang, J. Alcock, R. Fedosejevs, M. Blumin, I. Saveliev, S. Yang, H. Ruda, Y.Y. Tsui, Appl. Phys. B **87**, 671 (2007)
10. C. Honninger, R. Paschotta, F. Morier-Genoud, M. Moser, U. Keller, J. Opt. Soc. Am. B **16**, 46 (1999)
11. R. Paschotta, U. Keller, Appl. Phys. B **73**, 653 (2001)

12. S. De Silvestri, P. Laporta, O. Svelto, IEEE J. Quantum Electron. **20**, 533 (1984)
13. M. Moenster, U. Griebner, W. Richter, G. Steinmeyer, IEEE J. Quantum Electron. **43**, 174 (2007)
14. M. Lumb, E. Clarke, D. Farrell, M.J. Damzen, R. Murray, Mater. Res. Soc. Symp. Proc. **1076**, K09 (2008)
15. H.A. MacLeod, *Thin-Film Optical Filters*, 3rd edn. (Institute of Physics, Bristol, 2002)
16. S. De Silvestri, P. Laporta, O. Svelto, Opt. Lett. **9**, 335 (1984)
17. D.I. Babic, S.W. Corzine, IEEE J. Quantum Electron. **28**, 514 (1992)
18. D. Marcuse, Appl. Opt. **19**, 1653 (1980)
19. P. Laporta, V. Magni, Appl. Opt. **24**, 2014 (1985)
20. E. Sorokin, G. Tempea, T. Brabec, J. Opt. Soc. Am. B **17**, 146 (2000)
21. I.D. Jung, L.R. Brovelli, M. Kamp, U. Keller, M. Moser, Opt. Lett. **20**, 1559 (1995)
22. E.C. Le Ru, P. Howe, T.S. Jones, R. Murray, Phys. Rev. B **67**, 165303 (2003)
23. L. Zhang, T.F. Boggess, D.G. Deppe, D.L. Huffaker, O.B. Shchekin, C. Cao, Appl. Phys. Lett. **76**, 1222 (2000)
24. M. Sugawara, *Self-assembled InGaAs Quantum Dots* (Academic Press, San Diego, 1999)
25. D.J.H.C. Maas, A.R. Bellancourt, M. Hoffmann, B. Rudin, Y. Barbarin, M. Golling, T. Sudmeyer, U. Keller, Opt. Express **16**, 18646 (2008)
26. H.D. Sun, G.J. Valentine, R. Macaluso, S. Calvez, D. Burns, M.D. Dawson, T. Jouhti, M. Pessa, Opt. Lett. **27**, 2124 (2002)
27. V. Liverini, S. Schon, R. Grange, M. Haiml, S.C. Zeller, U. Keller, Appl. Phys. Lett. **84**, 4002 (2004)
28. Z. Zhang, K. Torizuka, T. Itatani, K. Kobayashi, T. Sugaya, T. Nakegawa, Opt. Lett. **22**, 1006 (1997)
29. V. Petrov, V. Shcheslavskiy, T. Mirtchev, F. Noack, T. Itatani, T. Sugaya, T. Nakagawa, Electron. Lett. **34**, 559 (1998)